Available online at www.sciencedirect.com
ScienceDirect
Journal of Catalysis 249 (2007) 79–92
JOURNAL OF CATALYSIS
www.elsevier.com/locate/jcat

FCC gasoline sulfur reduction additives: Mechanism and active sites

F. Can [a,1], A. Travert [a,*], V. Ruaux [a], J.-P. Gilson [a], F. Maugé [a], R. Hu [b], R.F. Wormsbecher [b]

[a] *Laboratoire Catalyse et Spectrochimie, UMR CNRS—ENSICAEN, 6, Blvd du Maréchal Juin, Université de Caen, 14050 Caen Cedex, France*
[b] *W.R. Grace & Co.-Conn., 7500 Grace Drive, Columbia, MD 21044, USA*

Received 2 February 2007; revised 29 March 2007; accepted 3 April 2007

Abstract

The interaction and reactivity of model sulfur compounds with gasoline sulfur reduction additives based on Zn-, Na-, and F-doped γ-Al_2O_3 have been investigated by in situ and operando infrared spectroscopy and microactivity tests. While gasoline sulfur reduction additives selectively crack tetrahydrothiophene (THT) into H_2S and butadiene they are inactive toward thiophene. When blended with a fluid catalytic cracking (FCC) catalyst, gasoline sulfur reduction additives do reduce (alkyl)thiophene contents in gasoline. There is a synergy between the FCC catalyst and the gasoline sulfur reduction additive leading to sulfur reduction. Under actual FCC conditions, Al_2O_3-based gasoline sulfur reduction additives reduce thiophenic compounds by decomposing (alkyl)THT formed via hydrogen transfer on the FCC catalyst. A balance between acid and base properties is required for an optimum activity of the additive, suggesting that THT cracking occurs on Lewis acid–base pairs through successive E2 eliminations.

Keywords: Fluid catalytic cracking; Gasoline sulfur reduction; Tetrahydrothiophene; Thiophene; Alumina; Acid–base properties

1. Introduction

As a result of environmental legislation on motor vehicles emissions, refiners face an increasing demand for fuels containing ever lower sulfur levels [1,2]. The production of gasoline by fluid catalytic cracking (FCC) units contributes to about 33% of the gasoline pool leaving a typical refinery and is responsible for about 90% of sulfur found in gasoline. The most important class of sulfur compounds in FCC gasoline consist in thiophenic species: thiophene, alkylthiophenes, and benzothiophene [3,4]. These compounds are not present in the virgin crude and are formed in the riser either by cracking of heavier sulfur compounds [5–7] or by recombination of H_2S with olefins [8]. Thiophenic compounds are very stable in FCC conditions [7], and it is generally admitted that their conversion requires previous hydrogenation by hydrogen transfer (HT) from H-donor molecules before cracking [6,9] (Scheme 1).

Although conventional hydrodesulfurization (HDS) of the FCC gasoline is an effective way to reduce the sulfur content, it decreases the octane number of the gasoline [10]. Other desulfurization processes (e.g., selective HDS, selective adsorption) minimize this octane loss, but they all require specific units (see [11–13] and references therein). Therefore, improving desulfurization within the FCC unit would be attractive, because it avoids pretreatment or post-treatment of the FCC charge or effluent in dedicated units (i.e., capital expenditure in a refinery). Modification of the FCC process parameters (e.g., riser temperature, cut points), although allowing a decrease in the sulfur content of the gasoline cut, strongly degrades yields and product quality [14,15]. For these reasons, gasoline sulfur re-

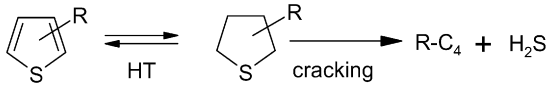

Scheme 1.

* Corresponding author. Fax: +33 2 31 45 28 22.
E-mail address: arnaud.travert@ensicaen.fr (A. Travert).
[1] Present address: LACCO, Université de Poitiers, 40, Av. du recteur Pineau, 86022 Poitiers, France.

0021-9517/$ – see front matter
doi:10.1016/j.jcat.2007.04.001

duction catalysts in the FCC unit have been proposed by Grace Davison [16–19] and are currently implemented in some refineries. This technology uses a solid Lewis acid supported on alumina (ZnO/Al_2O_3) as an additive at a level of about 10 wt% of the total FCC catalyst inventory. Laboratory microactivity tests (MAT) [5,20–22] or pilot plant tests (Davison circulating riser) [16–19] have shown that these additives could decrease the sulfur content of FCC gasoline by as much as 40% without significantly affecting other yields, excepting a slight increase of coke and hydrogen production [20]. However, such a sulfur removal in the FCC gasoline mostly concerns thiophene and light alkylthiophenes contents whereas heavier sulfur species such as benzothiophene are much less affected [5,16].

The mechanism by which gasoline sulfur reduction additives reduce thiophenic compounds has not yet been fully elucidated. Considering the above mentioned mechanism (Scheme 1), Harding et al. have proposed that gasoline sulfur reduction additives primarily enhance the rate of THT cracking to H_2S, thus preventing its conversion to thiophene by dehydrogenation reactions [9]. Alternatively, Andersson et al. [20] and Myrstad et al. [23] have suggested that gasoline sulfur reduction could be due to improved hydrogen transfer to thiophenic species initiated by the increase of coke production. More recently, Shan et al. [21] and Vargas-Tah et al. [24] have proposed that sulfur reduction occurs by strong adsorption of thiophenic species on Lewis acid sites of the additive and further cracking.

The objective of the present work is to identify the active sites and the reaction mechanisms by which alumina-based gasoline sulfur reduction additives eliminate thiophenic species. Toward this objective, acid–base properties of two γ-Al_2O_3 have been modified by sodium, zinc, and fluorine incorporation, then characterized by infrared (IR) spectroscopy of adsorbed probe molecules (pyridine and CO_2) and subsequently tested for thiophene and tetrahydrothiophene decomposition. Relationships between catalytic performance and the surface properties monitored under working conditions also have been established.

2. Experimental

2.1. Al_2O_3-based additives

Two commercial alumina samples, Catapal-C and Hi-Q, provided by Grace Davison (denoted Al_2O_3-C and Al_2O_3-HQ in what follows) were studied. These samples differ mainly in their Na content and their textural properties (Table 1). The surface properties of these parent aluminas were modified by doping them with sodium, zinc, and fluorine. Zinc was introduced on Al_2O_3-HQ by impregnation with $Zn(NO_3)_2$ as described previously [16]. The impregnated powder was dried overnight at 383 K, heated at 1088 K for 4 h, and steamed for 4 h at the same temperature. X-ray diffraction (XRD) patterns revealed the presence of $ZnAl_2O_4$. Sodium and fluorine were deposited on Al_2O_3-C by dry impregnation. An aqueous solution containing the appropriate amount of Na_2CO_3 and NH_4F was contacted with alumina. After 2 h of maturation at room temperature, the catalyst was dried at 393 K for 3 h before calcination under air (60 ml min^{-1}) up to 823 K for 3 h. XRD measurements showed that sodium and fluorine deposition did not modify the bulk structure of the alumina. The samples references and main characteristics are reported in Table 1.

Table 1
Surface area and composition of Al_2O_3-based additives

Additives	S_{BET} ($m^2\,g^{-1}$)	[Na] (wt ppm)	[Zn] (wt%)	[F] (wt%)
Al_2O_3-C	199	250	0	0
Na_{670}/Al_2O_3-C	184	670	0	0
Na_{1465}/Al_2O_3-C	192	1465	0	0
$F_{0.2}/Al_2O_3$-C	188	230	0	0.2
$F_{0.4}/Al_2O_3$-C	188	230	0	0.4
$F_{1.3}/Al_2O_3$-C	178	220	0	1.3
Al_2O_3-HQ	136	100	0	0
Zn/Al_2O_3-HQ	110	400	10	0

2.2. Characterization by IR spectroscopy

The additives were pressed into self-supported wafers (discs of about 20 mg, 2 cm^2) and activated in situ in the IR cell by heating up to 723 K under vacuum. Pyridine was adsorbed at room temperature (133 Pa at equilibrium) and further desorbed at 423 K under vacuum (10^{-4} Pa) for 15 min to eliminate physisorbed and H-bonded pyridine from the surface. In distinct experiments, carbon dioxide was adsorbed on the activated additives at room temperature (1330 Pa at equilibrium for 15 min). Known amounts of THT were added into the cell via a calibrated volume (1.75 cm^3) and the pressure was monitored by a gauge (0–1330 Pa).

IR spectra were recorded on a Nicolet Magna 750 IR spectrometer equipped with a DTGS detector and a KBr beam splitter using a resolution of 4 cm^{-1} and 126 scans. The spectra presented in this paper were normalized to a disc of 10 mg cm^{-2}.

2.3. Catalytic tests

2.3.1. Short contact time microactivity tests

Short contact time microactivity tests (SCT-MATs) [25] were carried out in an automated fixed-bed unit at 800 K, using a commercially available FCC catalyst from Grace Davison and the Zn/Al_2O_3-HQ additive blended at a level of 10 wt%. To simulate an equilibrium catalyst in a commercial unit, the catalyst and the additive were steamed separately in a fluidized bed for 4 h at 1088 K with 100% steam. After steaming, the FCC catalyst had a unit cell size 24.24 Å, a zeolite surface area of 181 $m^2\,g^{-1}$, and a matrix surface area of 31 $m^2\,g^{-1}$, whereas the steamed Zn/Al_2O_3-HQ additive had a surface area of 80 $m^2\,g^{-1}$.

Two model feeds were used: pure hexadecane (sulfur-free feed) and a mixture of hexadecane and 3-hexylthiophene (sulfur-containing feed) with a sulfur content of 1%, similar to that of a typical FCC feed. To vary the conversion, the catalyst-to-oil ratio was adjusted in the range of 4–8 g g^{-1} at a constant feed weight of 1.5 g and a constant feed injection time of 9 s.

After the cracking experiment, the coke on FCC catalyst was determined by a carbon analyzer as described previously [25].

Gas chromatography (GC) was used to analyze the products obtained from the cracking experiments, such as hydrogen, C1–C6 gases, gasoline, LCO, and bottom fractions and gasoline composition, as described previously [25]. The yields were calculated as weight percent of reactant. The fractions of gasoline and LCO were determined at cut points of 494 and 644 K (221 and 371 °C).

The gasoline sulfur concentration was analyzed using an Agilient 6890 gas chromatograph with an atomic emission detector G2350A using techniques similar to those described previously [26]. Product yield, gasoline composition, and sulfur content at constant conversion (63%) were obtained by interpolating experimental values.

2.3.2. Continuous-flow activity tests

Continuous-flow activity tests were carried out in a quartz tubular reactor and performed at atmospheric pressure. Catalyst samples (20 mg) were introduced into the microreactor and activated under a helium flow (25 ml min^{-1}) for 1 h at 723 K. The contact time was fixed to 3.2 g h mol^{-1} for tetrahydrothiophene and to 4.3 g h mol^{-1} for thiophene. Reactant and reaction products were analyzed online by GC, IR spectroscopy, and mass spectrometry (MS). The gas chromatograph was a Varian Star 3400CX equipped with a 30-m CP-SIL 5CB column, maintained at 393 K, and a flame ionization detector. The IR analysis of the reaction products was performed using a tubular cell designed for gas analysis equipped with KBr windows (path length 175 mm; internal diameter 19 mm). Analysis was also performed with a quadrupole mass spectrometer (OmniStar, Pfeiffer Vacuum) to detect H_2S ($m/z = 34$).

2.3.3. IR characterization in reaction conditions (operando analysis)

The IR study of the catalyst in working conditions was performed using a reactor-IR cell [27,28]. This device is particularly well suited for operando analysis, because products of the reaction and species formed on the catalyst surface in working conditions can be analyzed simultaneously. In the reactor-IR cell, THT was sent under flow ($W/F = 3.2$ g h mol^{-1}) on the catalyst under the form of a thin disc of about 20 mg (2 cm^2). In the reactor-IR cell, the reaction temperature was limited to 688 K, lower than that used in the quartz microreactor (723 K). The reactant and products were analyzed online by GC and MS. Surface species present on the catalyst were simultaneously characterized by IR spectroscopy.

3. Results

3.1. Surface properties of alumina-based additives

This section reports the effect of the dopes (Na, Zn, F) on the acid–base properties of alumina.

3.1.1. Hydroxyl groups

IR spectra of the alumina-based catalysts after activation at 723 K are presented in the region of ν(OH) vibrations in Fig. 1. After activation at 723 K, the IR spectra of Al_2O_3-C and Al_2O_3-HQ showed four main bands at about 3790, 3770, 3730, and 3685 cm^{-1} assigned to the various OH groups of alumina [29,30]. The overall intensity of these ν(OH) bands was significantly lower on Al_2O_3-HQ, due to its lower specific surface area (Table 1).

Na/Al_2O_3-C Sodium incorporation led to an overall decrease in intensity of the initial ν(OH) bands (Fig. 1B). In agreement with previous studies [31,32], those with the highest frequencies (3790 and 3770 cm^{-1}) were the most affected and almost disappeared at the highest sodium loading (1465 ppm). In addition, a shoulder at 3755 cm^{-1} (also present on Al_2O_3-C, which contains 250 ppm of Na) grew with increased sodium loading, related to the influence of Na^+ on OH groups [32].

Zn/Al_2O_3-HQ In the presence of zinc, the bands at 3792 and 3730 cm^{-1} decreased significantly, whereas that at 3772 cm^{-1} increased in intensity, and a new band at 3755 cm^{-1} appeared (Fig. 1C).

F/Al_2O_3-C Fluorine addition also significantly decreased the ν(OH) bands at 3792 and 3772 cm^{-1} (Fig. 1D). At the highest fluorine loadings, the ν(OH) band at 3685 cm^{-1} partially decreased, and a new ν(OH) band at 3720 cm^{-1} appeared.

3.1.2. Pyridine adsorption

Pyridine was adsorbed at room temperature (133 Pa at equilibrium) and further desorbed at 423 K to eliminate physisorbed and H-bonded pyridine from the surface. In such conditions, only pyridine coordinated to Lewis acid sites (LAS) was observed. Fig. 2 shows the IR spectra in the ν8a range. Two ν8a bands can be distinguished at 1624 and 1618 cm^{-1}, previously assigned to pyridine coordinated to tetrahedral Al^{3+} (strong LAS) and to both tetrahedral and octahedral Al^{3+} (medium to weak LAS) [33,34]. After evacuation at 523 K, only pyridine coordinated to the strongest acid sites (1624 cm^{-1}) was detected. The influence of the dopes on LAS strength was assessed using the ν8a frequency, which increases with increasing acid strength, whereas quantification of the LAS was obtained from the surface area of the ν19b band at about 1452 cm^{-1} using its molar absorption coefficient ($\varepsilon = 1.5$ cm µmol^{-1} [35]). The total amount of LAS was determined using the surface area of this band measured after evacuation at 423 K, whereas the strongest LAS was detected considering this band after evacuation at 523 K. These data are reported in Table 2.

Na/Al_2O_3-C Sodium addition decreased the total amount of Lewis acid sites. Fig. 2A illustrates that Na incorporation decreased the concentrations of both strong and medium acid sites (bands at 1624 and 1618 cm^{-1}, respectively). Table 2 shows that addition of 420 and 1215 ppm of Na on Al_2O_3-C (Na_{670}/Al_2O_3 and Na_{1465}/Al_2O_3, respectively) decreased the total concentration of LAS by 130 and 1360 µmol g^{-1}, respectively. This corresponds to the disappearance of ∼7 and ∼25 LAS per sodium atom added. These values are similar to those reported previously for various Na/Al_2O_3 samples [32]. In the case of strong LAS, Na poisoning was less effective, because the addition of 1 Na atom led to the disappearance of about 3 strong LAS for both samples.

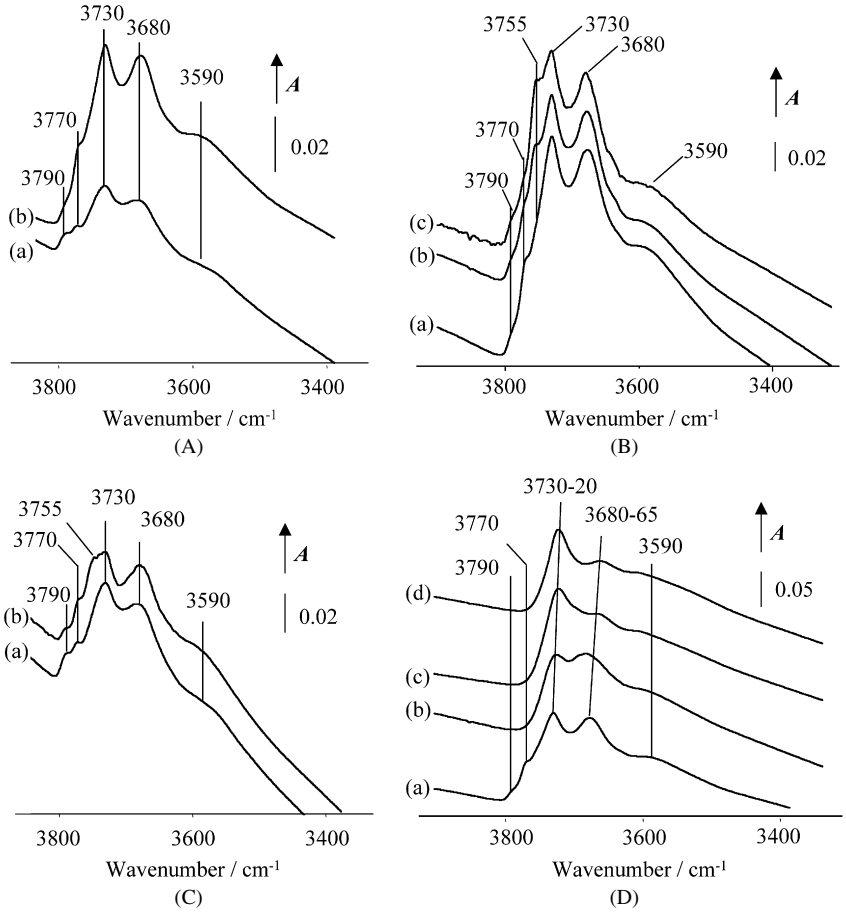

Fig. 1. IR spectra in the ν(OH) region of alumina-based additives activated at 723 K. (A) Parent aluminas: (a) Al_2O_3-C and (b) Al_2O_3-HQ; (B) Na-doped aluminas: (a) Al_2O_3-C, (b) Na_{670}/Al_2O_3-C, (c) Na_{1465}/Al_2O_3-C; (C) Zn-doped aluminas: (a) Al_2O_3-HQ, (b) Zn/Al_2O_3-HQ; (D) F-doped aluminas: (a) Al_2O_3-C, (b) $F_{0.2}/Al_2O_3$-C, (c) $F_{0.4}/Al_2O_3$-C, (d) $F_{1.3}/Al_2O_3$-C.

Zn/Al_2O_3-HQ Fig. 2B shows that zinc incorporation decreased the concentration of medium LAS characterized by the ν8a band at 1618 cm^{-1} but increases the LAS characterized by the band at 1624 cm^{-1} (Fig. 2B). Overall, the total concentration of LAS decreased, but the amount of strongest LAS increased significantly (Table 2). The results presented in Table 2 demonstrate that the introduction of about 50 Zn atoms leads to the creation of 1 strong Lewis acid site.

F/Al_2O_3-C The addition of fluorine increased the amount of both medium and strong LAS (Table 2). The creation of 1 strong Lewis acid site requires the introduction of about 5 fluorine atoms. It should be noted that no Brønsted acid sites were detected by pyridine on fluorinated samples.

3.1.3. Carbon dioxide adsorption

Fig. 3 shows the IR spectra recorded after CO_2 adsorption at room temperature (1330 Pa at equilibrium for 15 min). On Al_2O_3-C (Fig. 3A), carbon dioxide adsorption gave rise to bands at 3610, 1648, 1484, and 1235 cm^{-1}, characteristic of hydrogen-carbonate species (designated HC) formed by the interaction of CO_2 with basic OH groups [36]. Additional bands in the 1700–1850 cm^{-1} and 1150–1250 cm^{-1} ranges are assigned to bridged carbonate ions ("organic-like" species, designated OC), whereas the band at 1445 cm^{-1} is assigned to bidentate carbonates species (designated BC) [37]. A similar spectrum was obtained on Al_2O_3-HQ (Fig. 3B). The integrated intensities of the carbonate and hydrogen-carbonate bands in the 1940–1120 cm^{-1} range are reported in Table 2.

Na/Al_2O_3-C Na addition [samples Na_{670}/Al_2O_3 and Na_{1465}/Al_2O_3 (Fig. 3A)] did not modify the nature of species formed by CO_2 adsorption but did decrease the amount of hydrogen-carbonate and carbonate species.

Zn/Al_2O_3-HQ Addition of Zn led to slight decreases in initial carbonate and hydrogen-carbonate species (Fig. 3B). In addition, two sharp bands at 1624 and 1455 cm^{-1} were detected. On pure ZnO, carbonate species also gave rise to very sharp bands, but at different wavenumbers [38]. The two bands observed on Zn/HQ at 1624 and 1455 cm^{-1} are tentatively assigned to bidentate carbonate species adsorbed on Zn^{2+} cations of the spinel structure $Zn(AlO_2)_2$.

F/Al_2O_3-C On fluorinated alumina samples, carbonate and hydrogen-carbonate species similar to those observed on the parent Al_2O_3 (Al_2O_3-C) were also formed by CO_2 adsorption (Fig. 3C). However, the amounts of hydrogen-carbonate, bidentate carbonate, and organic carbonate species strongly decrease in the presence of fluorine.

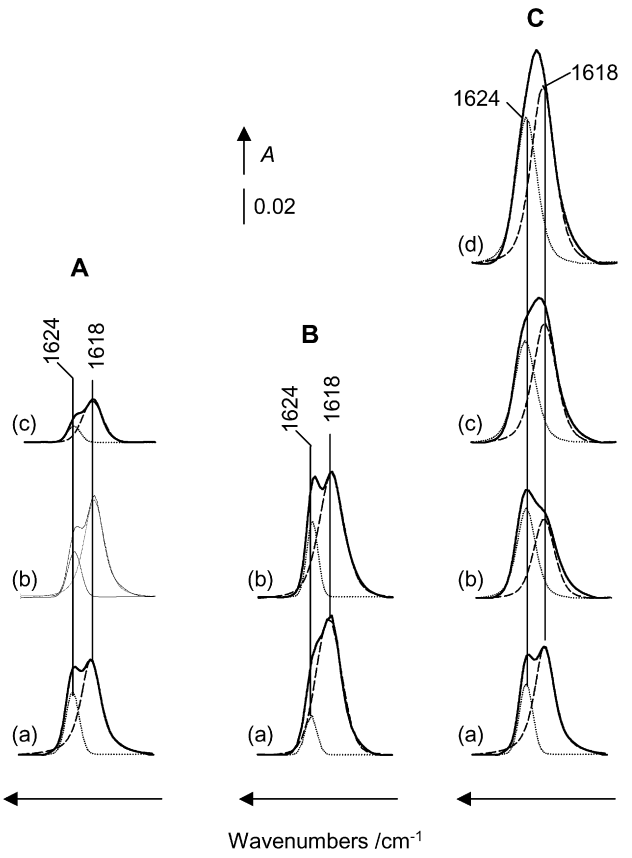

Fig. 2. ν8a-spectra of pyridine adsorbed on alumina-based catalysts at room temperature (1 Torr) followed by evacuation at 423 K. (A) Na-doped aluminas: (a) Al_2O_3-C, (b) Na_{670}/Al_2O_3-C, (c) Na_{1465}/Al_2O_3-C; (B) Zn-doped aluminas: (a) Al_2O_3-HQ, (b) Zn/Al_2O_3-HQ; (C) F-doped aluminas: (a) Al_2O_3-C, (b) $F_{0.2}/Al_2O_3$-C, (c) $F_{0.4}/Al_2O_3$-C, (d) $F_{1.3}/Al_2O_3$-C.

Table 2
Acid–base properties of Al_2O_3-based additives

Additives	Medium LAS[a] (μmol g^{-1})	Strong LAS[b] (μmol g^{-1})	Hydrogencarbonate + carbonate species[c] (au cm^{-1} mg^{-1})
Al_2O_3-C	1620	275	3.44
Na_{670}/Al_2O_3-C	1550	220	2.50
Na_{1465}/Al_2O_3-C	400	135	2.80
$F_{0.2}/Al_2O_3$-C	1650	280	1.90
$F_{0.4}/Al_2O_3$-C	1750	310	0.08
$F_{1.3}/Al_2O_3$-C	1930	440	0.04
Al_2O_3-HQ	1580	205	2.97
Zn/Al_2O_3-HQ	1350	240	2.18

[a] Coordinated pyridine after evacuation at 423 K.
[b] Coordinated pyridine after evacuation at 623 K.
[c] Specific integrated intensity of IR bands in the 1940–1120 cm^{-1} range.

3.2. THT and thiophene adsorption

The adsorption modes of THT and thiophene on Al_2O_3-based additives were studied. Fig. 4A shows the IR spectra recorded after adsorption of increasing amounts of THT on Al_2O_3-C activated at 723 K. THT adsorption led to the perturbation of the surface OH groups initially present and to the formation of a strong and broad ν(OH) band centered at

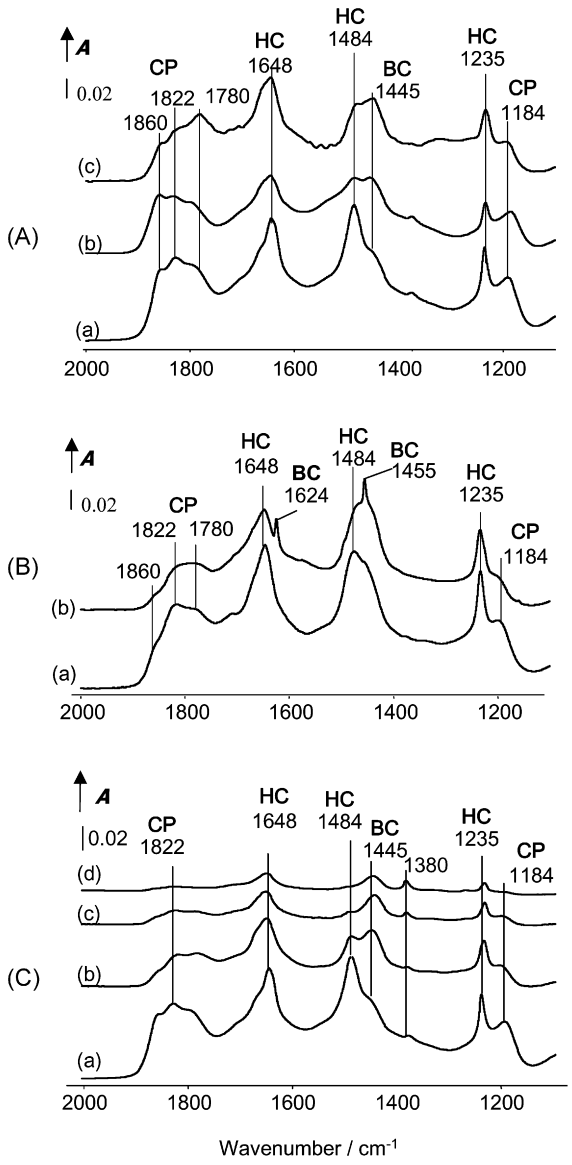

Fig. 3. IR spectra after CO_2 adsorption at room temperature on alumina-based catalysts activated at 723 K. (A) Na-doped aluminas: (a) Al_2O_3-C, (b) Na_{670}/Al_2O_3-C, (c) Na_{1465}/Al_2O_3-C; (B) Zn-doped aluminas: (a) Al_2O_3-HQ, (b) Zn/Al_2O_3-HQ; (C) F-doped aluminas: (a) Al_2O_3-C, (b) $F_{0.2}/Al_2O_3$-C, (c) $F_{0.4}/Al_2O_3$-C, (d) $F_{1.3}/Al_2O_3$-C. (HC: hydrogencarbonate; OC: organic carbonates; BC: bidentate carbonates.)

$\sim$3395 cm^{-1} resulting from their interaction with THT by hydrogen bonding. Adsorption of thiophene in similar conditions (not shown) also led to a perturbation of initial OH groups with a ν(OH) band due to hydrogen-bonded OH groups at $\sim$3605 cm^{-1}. This indicates that THT interacted more strongly than thiophene with the surface hydroxyl groups, due to its higher basicity (proton affinity, PA = 849 kJ mol^{-1}) compared with thiophene (PA = 815 kJ mol^{-1}) [39].

At low coverage, THT adsorbed on alumina Al_2O_3-C gave rise to two main ν(CH) bands at 2960 and 2871 cm^{-1}, shifting toward lower wavenumbers as the coverage increased (2953 and 2866 cm^{-1} at an equilibrium pressure of 133 Pa). In parallel, the δ(CH) bands, observed in the 1500–1100 cm^{-1} range [40], shifted by $\sim$1–2 cm^{-1} with increasing coverage.

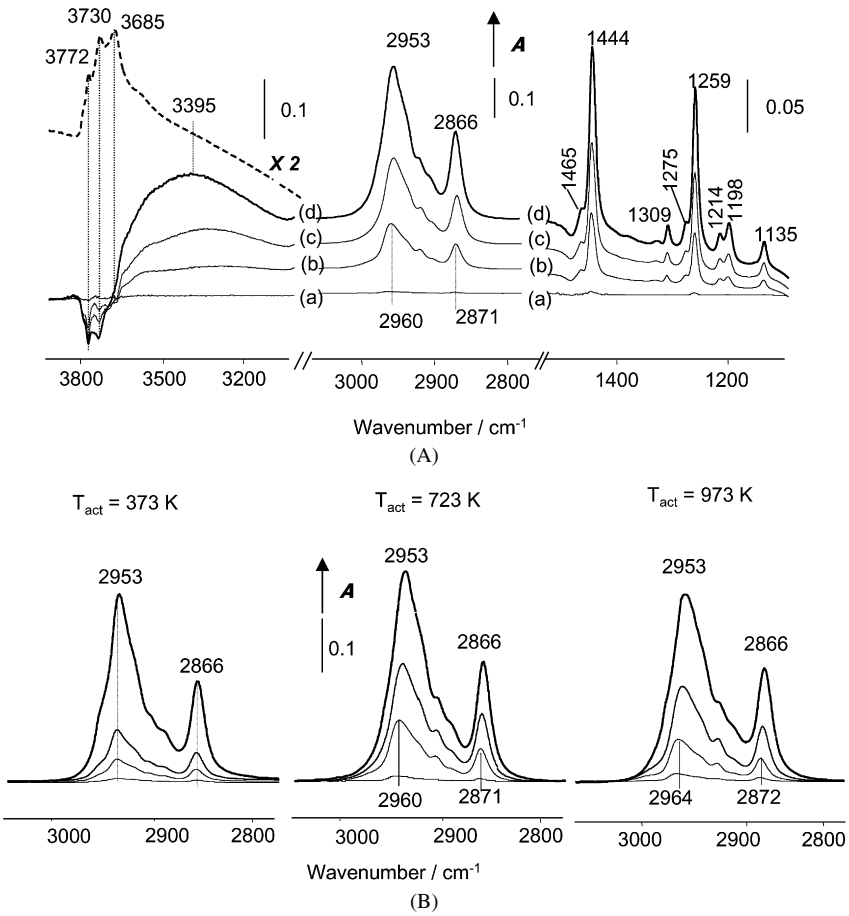

Fig. 4. (A) IR spectra after adsorption of increasing amounts of THT on Al_2O_3-C activated at 723 K (from (a) 10 μmol g^{-1} to (d) 133 Pa at the equilibrium). (B) ν(CH) spectra after adsorption of increasing amounts of THT on Al_2O_3-C activated at 373, 723, and 973 K.

On evacuation, both the ν(CH) and δ(CH) bands shifted toward higher wavenumbers. Conversely, the frequencies of the ν(C–C) vibrations of adsorbed THT (1000–1100 cm^{-1}) remained almost constant with the coverage. The observed ν(CH) and δ(CH) shifts could indicate a change in adsorption modes of THT as a function of the Al_2O_3 coverage.

To discriminate the various adsorption modes of THT, similar experiments were carried out on fully hydroxylated Al_2O_3-C (activated at 373 K [41]) and on Al_2O_3-C dehydroxylated at 973 K. Fig. 4B shows the corresponding ν(CH) spectra, the most sensitive to the THT coverage. On fully hydroxylated Al_2O_3-C, no shift of the ν(CH) bands can be seen, and the frequencies of the most intense bands are 2953 and 2866 cm^{-1}. This allows to assign such ν(CH) frequencies to hydrogen-bonded THT. Conversely, on Al_2O_3-C dehydroxylated at 973 K, the ν(CH) frequencies of adsorbed THT are seen at significantly higher frequencies at low coverage (2964 and 2872 cm^{-1}), shifting progressively toward 2953 and 2866 cm^{-1} with increasing coverage. It thus appears that the greater the dehydroxylation, the higher the ν(CH) frequencies at low coverage. This suggests that high ν(CH) frequencies observed at low coverage can be assigned to THT coordinated to Lewis acid sites of alumina. It is noteworthy that previous studies reported similar dependencies of ν(CH) frequencies on the adsorption mode of alcohols [42] and pyridine [43] on Al_2O_3. At higher THT coverage, the decreased ν(CH) frequencies can be explained by the interaction of THT with surface OH groups by hydrogen bonding. The reversibility of the ν(CH) frequency shift observed on evacuation indicates that THT preferentially interacts with Lewis acid sites of Al_2O_3-C. Similar results are obtained when THT was adsorbed on the other Al_2O_3-based additives used in this study.

The IR spectra recorded after thiophene adsorption on Al_2O_3-based catalysts (not reported here) were similar to those reported in the detailed study of Quigley et al. [44]. Examination of the ν(C=C) range (1400–1450 cm^{-1}) shows that like THT, thiophene adsorbed on Lewis acid sites as well as on OH groups of Al_2O_3 [44].

3.3. Cracking of a model feed

The gasoline sulfur reduction activity of the Zn/Al_2O_3-HQ additive was evaluated in a short-contact time microactivity test (SCT-MAT) fixed-bed unit at 798 K. The additive was blended with the steamed cracking catalyst (H-USY) at 10 wt%. Two model feeds were used, one sulfur-free (pure hexadecane) and the other spiked with 1% sulfur (hexadecane and 3-hexylthiophene), a level typical of FCC feeds. SCT-MAT was carried out at three different catalyst-to-oil ratios (3, 6, and 8), which led to conversions ranging from ca. 35 to ca. 70 wt%. Ta-

Table 3
Product yields and gasoline composition at constant conversion (63%)

Feed	Sulfur-free		Sulfur (1%)	
Catalyst	USY	USY + Zn/Al_2O_3-HQ	USY	USY + Zn/Al_2O_3-HQC
Cat/oil ratio (g/g)	7.4	8.0	6.2	6.7
Yields (wt%)				
Gas	27.6	26.8	24.9	25.4
Gasoline	35.1	34.4	35.4	35.4
LCO	36.6	36.8	35.9	35.9
Coke	0.71	1.09	0.56	0.91
Hydrogen	0.01	0.06	0.01	0.04
Gasoline composition (wt%)				
Paraffins	17.4	18.3	17.5	16.9
Isoparaffins	22.8	21.3	23.5	22.3
Aromatics	18.2	21.5	16.3	18.7
Naphthenes	3.6	3.6	3.9	3.6
Olefins	38.0	36.0	39.1	37.8

Table 4
Sulfur content and gasoline sulfur reduction at constant conversion (63 wt%)

	Sulfur content (ppm)		Sulfur reduction	
	USY	USY + Zn/Al_2O_3-C	ppm	%
Gasoline	2674	1982	692	26
LCO	6036	5698	338	6
Gasoline sulfur				
Mercaptans	18	16	2	11
THT	371	4	367	99
Thiophenol	34	26	8	23
Thiophene	408	350	58	14
Alkyl-thiophenes	1610	1339	271	17
Benzothiophene	233	242	−9	−4

ble 3 shows the product distribution at 63% conversion for both feeds, with or without the additive. In the presence of the additive, an increase in the catalyst/oil ratio by ∼10% was needed to maintain conversion, indicating that the additive, blended at a level of 10%, did not significantly affect conversion. Gasoline and LCO yields were not significantly affected by the additive. Only slight increases in coke, hydrogen, and gasoline aromatics occurred for both feeds when the additive was used. Similar trends were observed over the entire range of conversions (35–70%), in agreement with previous studies using real feeds [14].

The cracking of the sulfur feed yielded about 150 different sulfur compounds, from H_2S to alkyldibenzothiophenes. Table 4 shows the sulfur content of the gasoline and LCO fractions at 63% conversion. In the absence of additive, about 87% of the initial sulfur ended up in the gasoline range. Fig. 5 shows the sulfur content of gasoline and LCO evolution with conversion. Increasing the conversion led to decreased gasoline sulfur and increased LCO sulfur. Similar trends have been reported for real FCC feeds. On the other hand, the sulfur content of the gasoline was much higher than an FCC feed of similar sulfur content [14].

The additive led to a significant reduction in gasoline sulfur (−26%) and, to a lesser extent, in LCO sulfur (−6%, Table 3). The distribution of gasoline sulfur compounds at 63% conversion is shown in Table 4. Most of the gasoline sulfur reduction

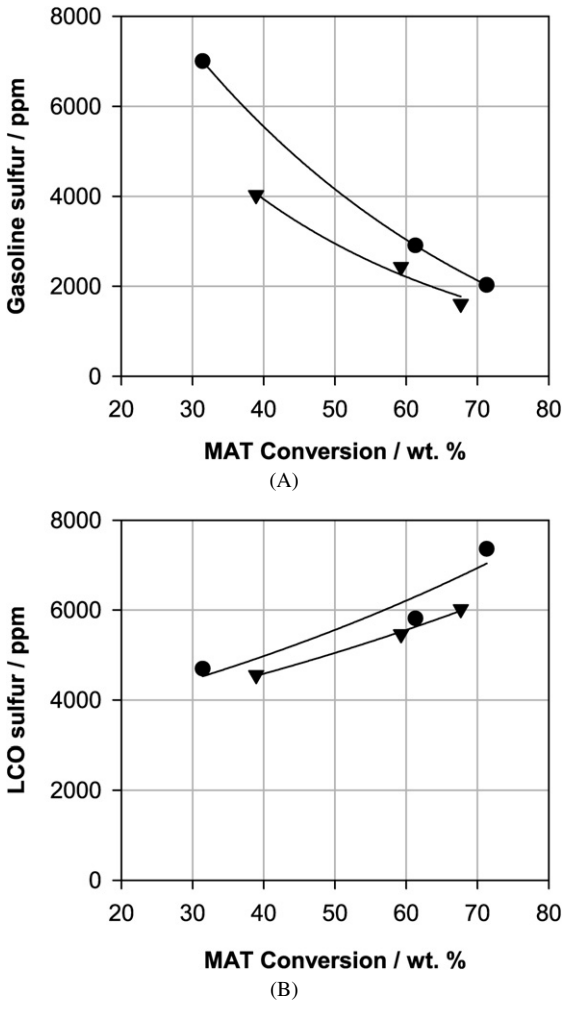

Fig. 5. Sulfur content of gasoline (A) and LCO (B) cuts versus conversion. (●) Cracking catalyst, (▼) cracking catalyst blended with Zn/Al_2O_3-C additive.

is accounted by the decreases in tetrahydrothiophene (THT), thiophene, and alkylthiophenes. In particular, the additive led to the complete elimination of THT, with much less thiophene reduction (∼−15%). Conversely, benzothiophene and most LCO

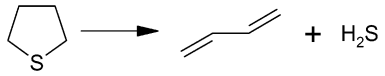

Scheme 2.

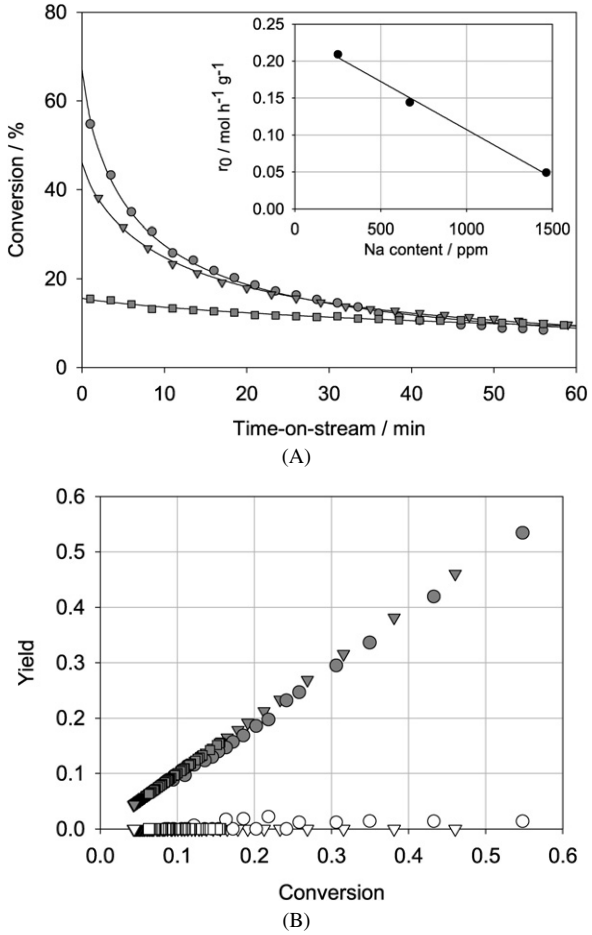

Fig. 6. Effect of Na on the conversion of THT at 723 K. (A) Conversion versus time on stream: (●) Al_2O_3-C, (▼) Na_{670}/Al_2O_3-C, and (■) Na_{1465}/Al_2O_3-C. Inset: initial conversion rate vs Na content. (B) Selectivity plots: full symbols, cracking; open symbols: dehydrogenation.

sulfur compounds (alkylbenzothiophenes and alkyldibenzothiophenes) were hardly affected by the additive.

3.4. Thiophene and THT reactivity on alumina-based additives

The reactivity of thiophene and THT was evaluated at 723 and 823 K on pure and doped-alumina samples. The contact times (W/F) were set to 4.3 and 3.2 g h mol^{-1} for thiophene and THT, respectively. Thiophene conversions were <1%. In contrast, in most of the additives, THT essentially cracked to 1,3-butadiene and H_2S according to the reaction, shown in Scheme 2.

This reaction is zero order with respect to THT. In addition, small amounts of dehydrogenation products (dihydrothiophenes and thiophene) were formed. As an example, Fig. 6A shows the evolution of the THT conversion on Al_2O_3-C and Na/Al_2O_3 additives as a function of the time on stream at 723 K; Fig. 6B shows the corresponding selectivity plots. The other Al_2O_3-based additives exhibited similar behaviors. As shown in Fig. 6A, the additives deactivate strongly with time on stream. To estimate the initial rates, the experimental data were fitted using the following empirical deactivation law: $r = r_0/(1 + At^{0.85})$, where A is a deactivation constant. Table 5 reports initial rates, deactivation constants, and cracking selectivities for the various additives, along with the initial rate and cracking selectivity obtained on H-Y zeolite for comparison.

Table 5
Initial rates, conversions, cracking selectivities and deactivation constant for THT transformation

	r_0 (mol h^{-1} g^{-1})	f_0 (%)	S_{crack} (%)	A (min$^{-0.85}$)
Al_2O_3-C	0.209	67.0	98	0.20
Na_{670}/Al_2O_3-C	0.144	46.1	100	0.12
Na_{1465}/Al_2O_3-C	0.049	15.6	100	0.02
$F_{0.2}/Al_2O_3$-C	0.090	28.9	94	0.21
$F_{0.4}/Al_2O_3$-C	0.059	18.9	91	0.12
$F_{1.3}/Al_2O_3$-C	0.010	3.2	100	0.01
Al_2O_3-HQ	0.115	36.8	96	0.16
Zn/Al_2O_3-HQ	0.170	54.5	96	0.27
H-Y	–	50.0[a]	35[a]	–

[a] Measured after 1 min of reaction.

As shown in Fig. 6A and Table 5, incorporation of sodium to Al_2O_3-C led to a marked decrease of the initial activity, and a linear relationship existed between the initial conversion and the Na content of the three additives (inset, Fig. 6A). In any case, cracking selectivity was not affected by Na and was very high (95%) for the three additives. Similarly, the addition of fluorine to Al_2O_3-C did not change the cracking selectivities but led to a very strong decrease in initial activity (Table 5), which became almost negligible for the highest fluorine content. Conversely, the addition of Zn to Al_2O_3-HQ increased the initial rate by about 50%. It is noteworthy that under our conditions, Zn did not modify THT cracking selectivities, whereas a slight increase in dehydrogenation products (e.g., coke, H_2) was reported from the use of this additive in the cracking of FCC feeds [20].

To assess the affect of the degree of dehydroxylation of Al_2O_3 on catalytic activity, Al_2O_3-C was activated at higher temperature (873 K vs 723 K) and then the reaction was also carried out under standard conditions (723 K). This increased activation temperature resulted in a significant increase in the initial conversion (87% vs 67%). To confirm the negative effect of hydroxylation, H_2S was added to the reactant flow (from 2 to 15 mol% H_2S). Under these conditions, *added* H_2S was in large excess compared with the H_2S *produced* by the reaction. On H_2S addition, a sharp decrease in activity occurred when up 7 mol% of H_2S was added. The addition of more H_2S did not produce any further activity decrease.

The H-Y zeolite was also active in THT conversion, but displayed a much lower selectivity toward cracking (35%) and yielded mainly dehydrogenation products. This is in line with a previous study of THT reactivity on an equilibrium FCC catalyst [8].

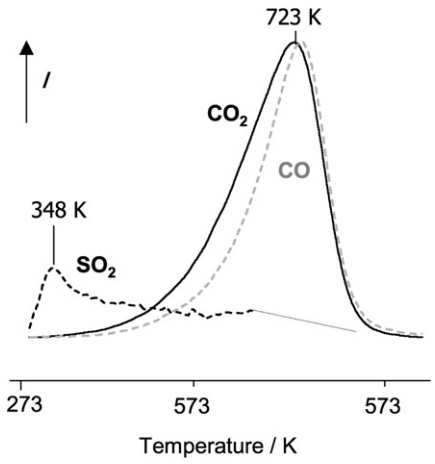

Fig. 7. Temperature-programmed oxidation of Al_2O_3-C after THT decomposition at 723 K during 1 h.

Finally, examination of Table 5 shows that the deactivation constant obtained for the various Al_2O_3-based additives increased roughly with the initial rate. This trend suggests that deactivation was due to a product. A chemical analysis of Al_2O_3-C carried out after 1 h of reaction indicated a carbon content of 4.6 wt% and a much smaller amount of sulfur (<0.3 wt%).

To gain more insight into the surface species remaining after reaction (1 h time on stream), temperature-programmed oxidation (TPO) was carried out after flushing with helium at 723 K and cooling to 323 K under helium. The additives were then regenerated under a flow of pure O_2 at increasing temperatures, up to 823 K. The oxidation products were analyzed by IR spectroscopy. As shown in Fig. 7, a single peak of SO_2 occurred at low temperature (∼348 K), whereas simultaneous production of CO and CO_2 occurred at much higher temperature (∼723 K). This suggests that carbon and sulfur deposits belong to distinct surface species. Initial activities were fully restored after regeneration of the additives.

3.5. Operando analysis of the reaction

To gain more insight into the nature of the active sites for THT cracking, the reaction was carried out in a transmission IR-reactor cell to simultaneously obtain the IR spectra of surface species and online measurement of catalytic activity. Because of the present specifications of the IR cell, the reaction had to be carried out at lower temperature (688 K) with the same contact time of the previous section (3.2 g h mol^{-1}). Consequently, the initial conversions were significantly lower (by a factor ∼6) than those measured in the quartz reactor. In any case, the relative activities of the additives toward THT were the same under both conditions.

3.5.1. Surface species under reaction conditions

The various additives show similar behaviors. As an example, a series of surface IR spectra recorded during the reaction of THT on Al_2O_3-C is displayed in Fig. 8A, and the evolution of the conversion with the time on stream is reported in Fig. 8B. The first spectra show a perturbation of surface OH groups and

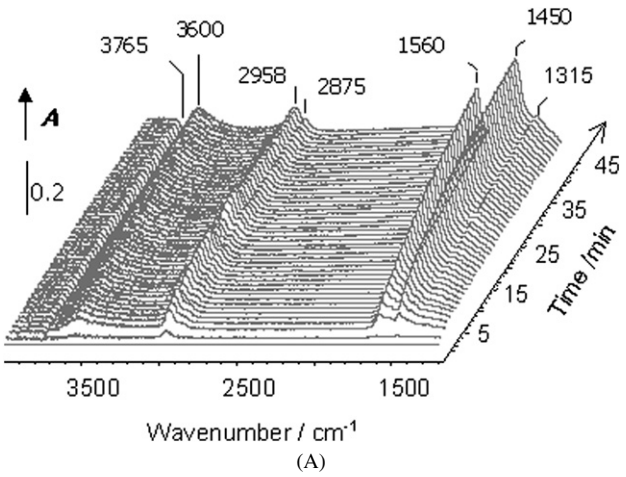

(A)

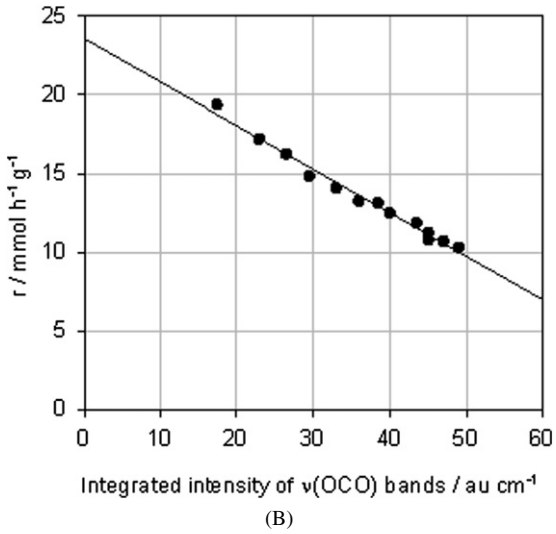

(B)

Fig. 8. (A) IR spectra recorded during THT conversion on Al_2O_3-C at 688 K. (B) THT conversion versus surface area of the carboxylate ν(OCO) bands.

the continuous growth of a broad ν(OH) band at ∼3600 cm^{-1}. This band is located at a much higher wavenumber than the broad ν(OH) band observed on THT adsorption at room temperature (3395 cm^{-1}; Fig. 4) and assigned to the hydrogen bonding of OH groups with THT. Such a large difference indicates that under reaction conditions (688 K), H-bonding of THT with surface OH groups would be unlikely. Moreover, the continuous growth of the ν(OH) band observed at 3600 cm^{-1} with the time on stream must be related to interaction of OH groups with surface species accumulating on the surface. These species gave rise to a group of ν(CH) bands in the 2970–2870 cm^{-1} range, two strong bands at 1565 and 1450 cm^{-1}, and a weaker band at 1315 cm^{-1} that grew continuously with the time on stream (Fig. 8A). Flushing of the catalyst with pure He at the reaction temperature decreased the ν(CH) bands slightly and restored a portion of the initial OH groups. Conversely, the strong bands at 1565 and 1450 cm^{-1} (characterizing surface species in strong interaction with the catalyst) were unaffected. These bands can be assigned to either coke or carboxylate species [45]. To ascertain their assignment, similar experiments (not shown) were carried out at 873 K in static conditions on alumina and on ^{18}O-exchanged alumina. The two strong bands

were downward-shifted by 9 and 20 cm^{-1} on ^{18}O-exchanged alumina compared with on nonexchanged alumina. Such shifts allow these bands to be unambiguously assigned to asymmetric and symmetric ν(OCO) stretching modes of surface carboxylate species [46].

Carboxylate species are known to be formed at high temperature on Al_2O_3 by a surface reaction involving unsaturated hydrocarbons such as ethylene [46], acetylene [45], butenes [47], or butadiene [48]. To verify whether 1,3-butadiene could be at the origin of the carboxylate species observed in the present study, the catalyst was contacted with 1,3-butadiene (150 Torr) in static conditions at high temperature (873 K) followed by evacuation at the same temperature. Similar ν(OCO) bands were formed, suggesting that carboxylate species could indeed be formed by a surface reaction of 1,3-butadiene, the major product of THT cracking. This is in agreement with TPO results showing that surface carbon species contained no sulfur (Fig. 7).

Fig. 8C shows the variation of THT conversion during the reaction as a function of the surface area of the carboxylate ν(OCO) bands, allowing evaluation of how carboxylate species affect catalytic activity. The linear correlation observed indicates that catalyst deactivation is likely due to the poisoning of active sites by carboxylate species.

3.5.2. *Influence of Lewis acid sites*

To modify the concentration of Lewis acid sites of the catalyst, various amounts of pyridine were adsorbed at 688 K before the reaction was performed. The IR spectra recorded after pyridine preadsorption (Fig. 9A) show that under such conditions, pyridine adsorbed only on the strongest LAS of alumina (ν8a band at 1624 cm^{-1}). The amount of LAS poisoned by pyridine adsorption can be determined from the area of the ν19b band (1452 cm^{-1}). The variation of the conversion in THT decomposition versus the amount of preadsorbed pyridine (Fig. 9B) shows that decreasing the concentration of strong LAS had a direct affect on catalytic activity.

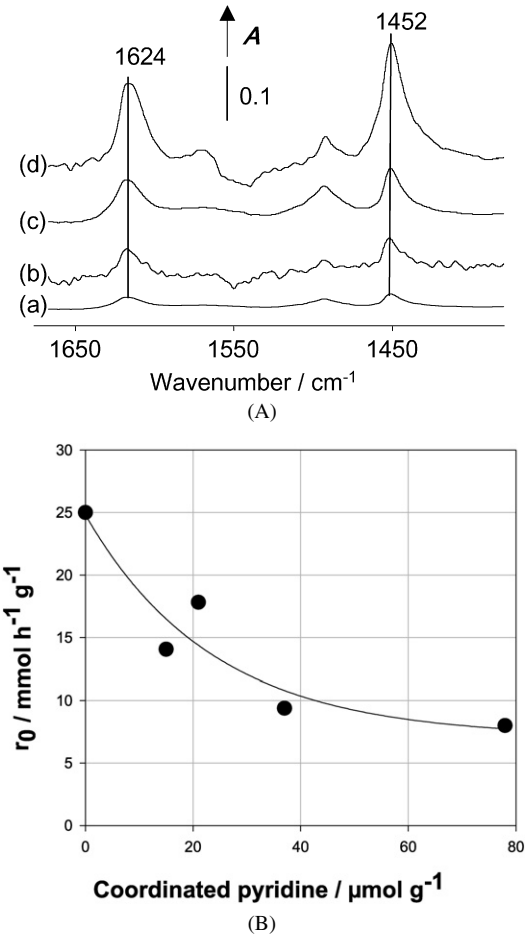

Fig. 9. Lewis acid sites poisoning by pyridine in operando condition at 688 K. (A) IR spectra recorded after pyridine preadsorption (a) 15 µmol/g, (b) 22 µmol/g, (c) 37 µmol/g, and (d) 78 µmol/g. (B) Initial conversion rate of versus the amount coordinated pyridine.

4. Discussion

4.1. *Role of gasoline sulfur reduction additives in sulfur elimination*

The SCT-MATs carried out on model feeds demonstrated that the Zn/Al_2O_3-HQ additive did not significantly affect conversion but slightly increased yields of coke, hydrogen, and aromatics (Table 3). This finding is in agreement with previous studies carried out on FCC feeds using similar gasoline sulfur reduction additives [5,14,20–22]. In the present case, however, the amount of gasoline sulfur was significantly higher than that obtained from FCC feeds of similar sulfur content. This is accounted for by the nature of the model sulfur molecule (3-hexylthiophene), converted mainly into thiophene and light alkylthiophenes belonging to the gasoline cut [8,9]. It is noteworthy that in the absence of the additive, the amount of THT formed in the gasoline cut was much higher than that usually observed for FCC feeds. In the presence of the additive, however, almost complete removal of THT occurred (Table 4). This contradicts the recent proposal of Andersson et al. [20] and Myrstad et al. [23], who linked gasoline sulfur reduction to improved hydrogen transfer to thiophenic species; in such a case, the amount of THT should be higher in the presence of the additive (Scheme 1). The relatively large amount of THT in the absence of additive demonstrates that under our conditions, the limiting factor for gasoline sulfur removal by the cracking catalyst (USY) was not the hydrogen transfer to thiophenic species, but rather the cracking of THT itself. Continuous-flow experiments showed that on H-Y zeolite, THT mainly undergoes dehydrogenation reactions leading to thiophene (65%) and, to a lesser extent, cracking reactions leading to H_2S and hydrocarbons (35%, Table 5). Similar selectivities have been reported by Leflaive et al. [8] for an equilibrium FCC catalyst. Conversely, the most active Al_2O_3-based additives (Al_2O_3-C and Zn/Al_2O_3-HQ) led to THT conversions of the same order of magnitude as obtained with H-Y zeolite, but were much more selective for THT cracking (>97%). Moreover, Al_2O_3-based additives showed very low activity toward thiophene compared with THT, indicating that direct desulfurization of thiophenic species by such additives (as recently proposed by Shan et al. [21] and Vargas-Tah et al. [24]) was unlikely.

Consequently, we conclude that the key role of Al_2O_3-based gasoline sulfur reduction additives is to selectively enhance the rate of THT cracking to butadiene and H_2S, thus preventing its conversion to thiophene by dehydrogenation reactions. Such a mechanism, initially proposed by Harding et al. [9], clearly explains the complete removal of THT as well as the significant decrease in (alkyl-)thiophene species when the gasoline sulfur reduction additive is blended to the cracking catalyst (Table 4).

In the case of real FCC feeds, the affect of process parameters on sulfur elimination has been examined previously [14]. They have been found to affect sulfur reduction as well as the main yields and product quality. Thus, improving hydrogen transfer by using RE-USY catalysts lowers the gasoline sulfur level, but also decreases olefins and the octane number [14], limiting the use of such high-hydrogen catalysts for sulfur reduction. In contrast, gasoline sulfur reduction additives do not significantly modify yields and product quality, and they improve sulfur reduction, even with RE-USY catalysts. Overall, gasoline sulfur reduction additives lead to increased hydrogen transfer to thiophenic species by preventing THT dehydrogenation. In contrast with RE-USY, this hydrogen transfer improvement is selective for thiophenic species.

4.2. Active sites for THT cracking by gasoline sulfur reduction additives

4.2.1. Acid sites

The facts that THT adsorption occurred preferentially on LAS (Fig. 4) and that selective poisoning of the strongest LAS significantly decreased the activity (Fig. 9) indicate that these sites play key roles in THT cracking. Because the doping of Al_2O_3 by sodium, zinc or fluorine changes the number and strength of Lewis acid sites, significant variations in the activities of doped Al_2O_3 can be expected. Fig. 10 shows the initial THT conversion versus the concentration of strong Lewis acid sites measured by pyridine (Table 2). The linear correlation obtained for the Na/Al_2O_3-C and Zn/Al_2O_3-HQ series of additives suggests that their activity is governed mainly by the variations in the amount of strong Lewis acid sites (Fig. 10A). No correlation between the activity of these additives and the amount of weak or (weak + strong) Lewis acid sites can be observed. The surface densities of the strong LAS of bare aluminas (Al_2O_3-C and Al_2O_3-HQ) are close (1.4 and 1.5 μmol m^{-2}, respectively), indicating that variation in their initial activity is related mainly to the difference in their surface areas (Table 1).

Conversely, Na doping did not significantly change surface area, but did induce a significant decrease in both Lewis acidity and THT cracking activity. Sodium is a known poison of alumina for many reactions, including alcohol dehydration [32,49,50], olefin isomerization [49], cumene cracking [51], and catalytic oxidation [52]. The adverse effect of sodium on gasoline sulfur reduction additives in FCC also has been reported recently [19]. This effect is generally explained as a decrease in the number and strength of Lewis acid sites on sodium addition [32,53,54]. In agreement with the findings of Saad et al. [32], our results indicate that the amount of poisoned Lewis acid sites on alumina was significantly higher than the amount

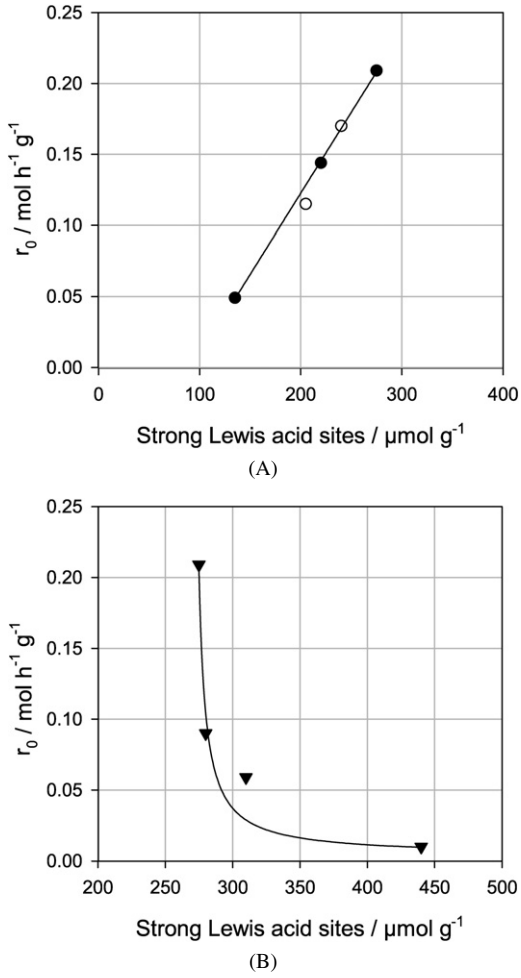

Fig. 10. Initial THT conversion rate versus the concentration of strong Lewis acid sites of alumina-based additives as measured by pyridine adsorption. (A) Na-doped (○) and Zn-doped (●) additive. (B) F-doped additives (▼).

of added Na^+ cations (Table 2). This can be explained by inductive effects from Na^+ ions localized on surface cation vacancies [32,54].

The addition of Zn to Al_2O_3 led to opposite effects, because both the amount of strong LAS and the initial activity were increased. The nature of LAS on Zn/Al_2O_3-HQ did not differ significantly from those of the parent alumina, because coordinated pyridine species gave rise to similar IR spectra with ν8a bands at 1618 and 1624 cm^{-1}. The expected ν8a frequency for pyridine coordination on Zn^{2+} was at ∼1605 cm^{-1}, as reported for pyridine adsorption on pure ZnO [36]. This indicates that the LAS of Zn/Al_2O_3-HQ consisted mainly of coordinatively unsaturated Al^{3+} ions, in agreement with previous studies carried out on similar materials [24,55,56]. It is noteworthy that on an atomic basis, the effect of Zn was somewhat limited, because the creation of one strong LAS required the addition of about 50 Zn^{2+} ions. This implies that an important fraction of the Zn probably was not located on the surface, but was engaged in the formation of $ZnAl_2O_4$, as detected by XRD. Whereas in γ-Al_2O_3, Al^{3+} cations are distributed over both types of sites [57], in the normal spinel structure of $ZnAl_2O_4$, Zn and Al occupy octahedral and tetrahedral sites, respectively [58].

This can explain why $ZnAl_2O_4$ formation increases the amount of strong LAS (ν8a at 1624 cm^{-1}, tetrahedral Al sites [34]) at the expense of weaker LAS (ν8a at 1618 cm^{-1}, involving octahedral Al sites [34]).

The behavior of F-doped additives differed from that of Na- or Zn-doped aluminas. Fluorine increased the amount of strong LAS but decreased the initial activities in THT cracking (Fig. 10B). This increased Lewis acidity on fluorine incorporation is in agreement with previous findings [59–61]. It is generally believed that at low loadings, F^- ions substitute μ_1-OH groups, as indicated by the significant decrease in ν(OH) bands at 3790 and 3770 cm^{-1} (Fig. 1C). The increase in strong Lewis acid sites is usually associated with the higher electronegativity of the F^- ion compared with the OH^- ion, leading to a strengthening of vicinal Lewis acid sites. It should be noted that increased Brønsted acidity on fluorinated aluminas has been reported previously [60,61], but was not observed in the present work; however, in those studies the fluorine content was significantly higher than that used in the present work (0.2–1.3 wt%).

In view of the correlation established between Lewis acidity and THT cracking activity for Na- and Zn-doped aluminas (Fig. 10A), the low activity of F/Al_2O_3-C samples is surprising, especially because F is a known promoter of Lewis acid-catalyzed reactions [62]. This clearly indicates that Lewis acidity alone does not account for THT cracking on Al_2O_3-based additives.

4.2.2. Basic sites

The introduction of fluorine dramatically decreases the amount of basic OH groups and basic oxygen centers, as indicated by the low amount of hydrogen carbonate and carbonate species formed on CO_2 adsorption, respectively (Fig. 3; Table 2). To the best of our knowledge, no previous study has reported the influence of fluorine on the basic properties of Al_2O_3. The formation of hydrogen carbonate species is known to involve mainly μ_1-OH groups [36]. The significant decrease in hydrogen carbonate species thus can be accounted for by the progressive substitution of μ_1-OH groups by F^- ions reported above (Fig. 1C). Conversely, the decrease in carbonate species cannot be explained by a substitution of basic oxygen ions by F^- ions, which is observed only at fluorine contents greater than those used in the present work (>3 wt%) [63]. On the other hand, the electron-withdrawing inductive ($-I$) effect of F^- should lead to a weakening of the basicity of vicinal surface oxygen ions, explaining the significantly decreased carbonate species formation.

Fig. 11 shows the relationship between the initial activities of F/Al_2O_3-C additives in THT cracking and the amount of surface basic oxygen centers estimated from the integrated intensity of ν(CO) bands of carbonate and hydrogen carbonate species formed by CO_2 adsorption (Table 2). This linear correlation is a strong indication of the involvement of basic centers (surface O^{2-} anions or μ_1-OH groups) on F/Al_2O_3-C additives in THT cracking.

On Na/Al_2O_3-C additives, the amount of carbonate and hydrogen carbonate species decreased for the Na_{670}/Al_2O_3-C sample but increased for the Na_{1650}/Al_2O_3-C sample (Table 2). This finding agrees with a previous study [31] and has been linked to the migration of part of Na^+ ions into the bulk of Al_2O_3 at low sodium content (<1000 ppm), leading to a decrease in negatively charged surface basic centers [31]. At higher sodium content, basicity increased further when Na^+ migration to the bulk no longer occurred [31].

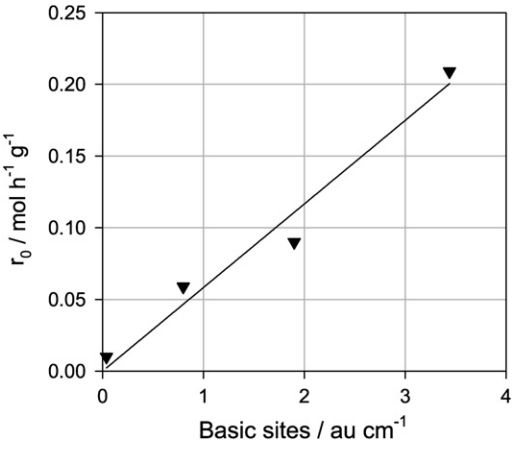

Fig. 11. Influence of the number of basic surface oxygen centers (evaluated from the total area of carbonate ad hydrogen carbonate IR bands) of F-doped aluminas on initial THT conversion rate.

The addition of Zn to Al_2O_3 led to the formation of peculiar bidentate carbonate species by CO_2 adsorption, characterized by two sharp $\nu(CO_2)$ bands at 1624 and 1455 cm^{-1} (Fig. 3C). Overall, however, decreased amounts of carbonate and hydrogen carbonate species formed on CO_2 adsorption were observed (Table 2). Thus, the relationship between initial activity and surface basicity observed for the F/Al_2O_3-C series of additives (Fig. 11) does not hold for Na- and Zn-doped additives, and it appears that both Lewis acid and basic properties account for the THT cracking activity of Al_2O_3-based additives.

Further insight into the nature of the active sites for THT cracking is provided by the IR spectra recorded under reaction conditions showing that catalyst deactivation is due to the formation of carboxylate species (Fig. 8). In agreement with a previous study, we found that such species can be formed by a secondary surface reaction involving 1,3-butadiene, the major product of THT cracking. These findings are consistent with the fact that faster deactivation was observed for the most active additives (Table 3). Although detailed mechanisms have been proposed for the formation of carboxylate species on Al_2O_3 from alcohols or aldehydes [64], much less is known about their formation from olefins. They could be formed by a reaction involving allylic complexes formed on (Al^{3+}, O^{2-}) pairs [47] and basic μ_1-OH groups [45]. In any case, the formation of carboxylate species from butadiene leads to the consumption of surface oxygen centers in the form of O^{2-} ions or basic OH groups. The linear decrease in catalytic activity with the amount of carboxylate species formed during the reaction (Fig. 8) thus provides another indication of the involvement of basic centers in the cracking of THT by Al_2O_3-based additives.

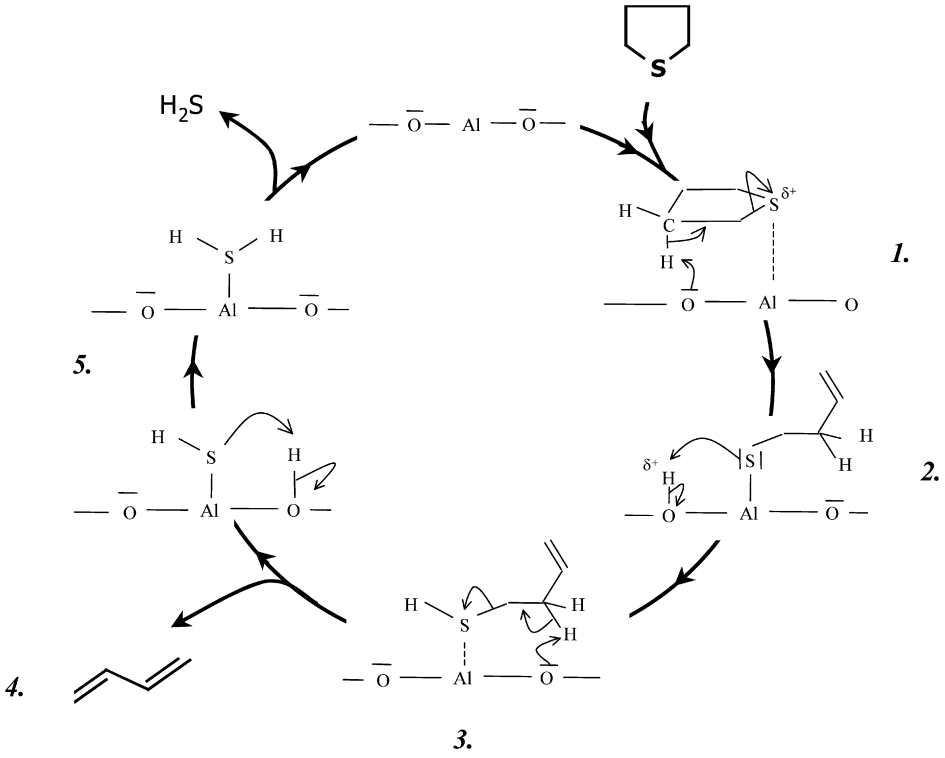

Fig. 12. Mechanism for tetrahydrothiophene decomposition on alumina-based additives.

4.2.3. Mechanism of THT cracking by Al_2O_3-based gasoline sulfur reduction additives

THT cracking presents strong similarities with the dehydration of alcohols on alumina in olefins and water. In particular, both reactions require acid and basic centers and show comparable sensitivities toward sodium [32,49,50]. It is generally believed that alcohol dehydration on Al_2O_3 follows a E2-type elimination mechanism involving Lewis acid–base pairs [65–69]. Accordingly, we propose the reaction mechanism depicted in Fig. 12, in which the basic sites (O) may be the oxygen atoms of the μ_1-OH group or O^{2-} anions and the acid sites (Al) are coordinatively unsaturated tetrahedral Al^{3+} sites. The coordination of THT to a strong Lewis acid site is expected to polarize the C–S bond, making possible the concerted proton abstraction in β-position by a vicinal basic site and the C–S bond cleavage, leading to a surface thiolate (step 1). The formation of butadiene requires recombination of thiolate with a proton (step 2) into a thiol, which in turn undergoes a second E2 elimination (step 3). The intermediate thiol (but-3-ene-1-thiol), which is less stable and presumably more reactive than THT, is not observed in the gas phase. Finally, H_2S is formed by recombination of the surface –SH groups with a proton (step 4). Both butadiene and H_2S may further react with the surface, leading to both carboxylate species and surface –SH groups. The formation of such surface species is fully consistent with the TPO profiles observed after the reaction (Fig. 7).

Finally, the proposed mechanism accounts for the high sensitivity of THT cracking toward modification of surface acid–base properties. In particular, it demonstrates that balanced acid–base pairs are required for optimum activity.

5. Conclusion

This contribution reports a study of acid–base properties and activities of Zn-, Na-, and F-doped Al_2O_3 on the desulfurization of model sulfur compounds. All three additives are inactive in thiophene conversion by themselves but selectively crack tetrahydrothiophene (THT) into H_2S and butadiene in the following order of activity: $Zn/Al_2O_3 > Al_2O_3 > Na/Al_2O_3 > F/Al_2O_3$. In contrast, when blended with a FCC catalyst, the Zn/Al_2O_3 additive catalyzes a significant conversion of both THT and (alkyl)thiophene, leading to a significant decrease in their content in the gasoline fraction. This illustrates that Al_2O_3-based gasoline sulfur reduction additives reduce thiophenic compounds by an efficient decomposition of THT produced by hydrogen transfer on an FCC catalyst.

THT cracking requires both Lewis acid and basic sites. The involvement of strong tetrahedral Al^{3+} sites has been demonstrated by specific poisoning using pyridine in operando conditions. A strong indication that basic sites are also involved in the reaction mechanism is the fact that deactivation originates from the formation of carboxylate species, leading to a blocking of surface oxygen centers.

The promoter effect of Zn on THT cracking has been assigned to formation of the spinel $ZnAl_2O_4$ favoring the formation of strong tetrahedral Al^{3+} acid sites at the expense of medium octahedral Al^{3+} acid sites. Conversely, Na leads to a significant decrease in the number of strong Lewis acid sites by inductive effects, thus explaining the lower activity of Na/Al_2O_3 additives. Fluorine enhances strong Lewis acid sites, but also strongly decreases surface basicity through substitution of μ_1-OH groups and electron-withdrawal from surface O^{2-}

centers. In this case, Lewis basicity becomes the limiting factor for THT cracking.

Overall, our results demonstrate that a good balance of the acid–base properties is required for optimum activity, suggesting that THT cracking occurs on Lewis acid–base pairs through successive E2 elimination.

References

[1] US Environmental Protection Agency, Federal Register 65 (2000) 6698.
[2] European Parliament and Council of the European Union, Official J. Eur. Union L 176 (2003) 10.
[3] R.R. Gatte, R.H. Harding, T. Albro, D. Chin, R.F. Wormsbecher, Am. Chem. Soc. Prepr. Div. Pet. Chem. 37 (1992) 33.
[4] C. Yin, D. Xia, Fuel 83 (2004) 433.
[5] A. Corma, C. Martinez, P. Gullbrand, Am. Chem. Soc. Prepr. Div. Pet. Chem. 44 (1999) 490.
[6] A. Corma, C. Martinez, G. Ketley, G. Blair, Appl. Catal. A Gen. 208 (2001) 135.
[7] X. Dupain, L.J. Rogier, E.D. Gamas, M. Makkee, J.A. Moulijn, Appl. Catal. A Gen. 238 (2003) 223.
[8] P. Leflaive, J.L. Lemberton, G. Perot, C. Mirgain, J.Y. Carriat, J.M. Colin, Appl. Catal. A Gen. 227 (2002) 201.
[9] R.H. Harding, R. Gatte, J.A. Whitecavage, R.F. Wormsbecher, in: J.N. Armor (Ed.), Environmental Catalysis, American Chemical Society, Washington, DC, 1994, p. 286.
[10] J.P. Greeley, S. Zaczepinski, T.R. Halbert, G.B. Brignac, A.R. Gentry, S. Mayo, in: NPRA 1999 Annual Meeting, AM-99-31, San Antonio, TX, March 21–23, 1999.
[11] C. Song, X. Ma, Appl. Catal. B Environ. 41 (2003) 207.
[12] I.V. Babich, J.A. Moulijn, Fuel 82 (2003) 607.
[13] S. Brunet, D. Mey, G. Perot, C. Bouchy, F. Diehl, Appl. Catal. A Gen. 278 (2005) 143.
[14] R.F. Wormsbecher, G.D. Weatherbee, G. Kim, T.J. Dougan, in: NPRA 1993 Annual Meeting, AM-93-55, San Antonio, TX, March 21–23, 1993.
[15] E.T. Habib Jr., X. Zhao, G. Yaluris, W.C. Cheng, L.T. Boock, J.P. Gilson, in: M. Guisnet, J.P. Gilson (Eds.), Zeolites for Cleaner Technologies, Imperial College Press, 2002, p. 105.
[16] R.F. Wormsbecher, G. Kim, US Patent 5,376,608 (1994), to W.R. Grace & Co.-Conn.
[17] R.F. Wormsbecher, G. Kim, US Patent 5,525,210 (1996), to W.R. Grace & Co.-Conn.
[18] X. Zhao, W.-C. Cheng, J.A. Rudesill, R.F. Wormsbecher, P.S. Deitz, US Patent 6,635,168 (2003), to W.R. Grace & Co.-Conn.
[19] R. Hu, X. Zhao, R.F. Wormsbecher, M.S. Ziebarth, US Patent Application 2005/0205464 (2005), to W.R. Grace & Co.-Conn.
[20] P.O.F. Andersson, M. Pirjamali, S.G. Jaras, M. Boutonnet-Kizling, Catal. Today 53 (1999) 565.
[21] H.H. Shan, C.Y. Li, C.H. Yang, H. Zhao, B.Y. Zhao, J.F. Zhang, Catal. Today 77 (2002) 117.
[22] M.A.B. Siddiqui, S. Ahmed, A.M. Aitani, C.F. Dean, Appl. Catal. A Gen. 303 (2006) 116.
[23] T. Myrstad, H. Engan, B. Seljestokken, E. Rytter, Appl. Catal. A Gen. 187 (1999) 207.
[24] A.A. Vargas-Tah, R.C. Garcia, L.F.P. Archila, J.R. Solis, A.J.G. Lopez, Catal. Today 107–108 (2005) 713.
[25] D. Wallenstein, U. Alkemade, Appl. Catal. A Gen. 137 (1996) 37.
[26] T.G. Albro, P.A. Dreifuss, R.F. Wormsbecher, J. High Resolut. Chromatogr. 16 (1993) 13.
[27] A. Travert, F. Maugé, Stud. Surf. Sci. Catal. 127 (1999) 269.
[28] J.F. Joly, N. Zanier-Szydlowski, S. Colin, F. Raatz, J. Saussey, J.C. Lavalley, Catal. Today 9 (1991) 31.
[29] H. Knözinger, P. Ratnasamy, Catal. Rev. Sci. Eng. 17 (1978) 31.
[30] M. Digne, P. Sautet, P. Raybaud, P. Euzen, H. Toulhoat, J. Catal. 226 (2004) 54.
[31] V.A. Ivanov, A. Piéplu, J.C. Lavalley, P. Nortier, Appl. Catal. A Gen. 131 (1995) 323.
[32] A.B.M. Saad, V.A. Ivanov, J.C. Lavalley, P. Nortier, F. Luck, Appl. Catal. A Gen. 93 (1993) 71.
[33] F. Abbatista, S. Delmasko, G. Gozzelino, D. Mazza, M. Vallino, G. Busca, V. Lorenzelli, G. Ramis, J. Catal. 117 (1989) 42.
[34] C. Morterra, G. Magnacca, Catal. Today 27 (1996) 497.
[35] S. Khabtou, T. Chevreau, J.-C. Lavalley, Microporous Mater. 3 (1994) 133.
[36] J.C. Lavalley, Catal. Today 27 (1996) 377.
[37] C. Morterra, A. Zecchina, S. Coluccia, J. Chem. Soc. Faraday Trans. I 73 (1977) 1544.
[38] J. Saussey, J.C. Lavalley, C. Bovet, J. Chem. Soc. Faraday Trans. I 78 (1982) 1457.
[39] E.P. Hunter, S.G. Lias, J. Phys. Chem. Ref. Data 27 (1998) 413.
[40] T.M. El-Gogary, Spectrochim. Acta A 57 (2001) 1405.
[41] A.A. Tsyganenko, K.S. Smirnov, A.M. Rzhevskij, P.P. Mardilovich, Mater. Chem. Phys. 26 (1990) 35.
[42] J. Caillod, J.C. Lavalley, J. Chem. Phys. 77 (1980) 379.
[43] A. Travert, A. Vimont, A. Sahibed-Dine, M. Daturi, J.-C. Lavalley, Appl. Catal. A Gen. 307 (2006) 98.
[44] W.W.C. Quigley, H.D. Yamamoto, P.A. Aegerter, G.J. Simpson, M.E. Bussell, Langmuir 12 (1996) 1500.
[45] J. Datka, Z. Sarbak, R.P. Eischens, J. Catal. 145 (1994) 544.
[46] J. Najbar, R.P. Eischens, in: Proceedings of the 9th International Congress on Catalysis, 1988, p. 1434.
[47] M. Trombetta, G. Busca, S.A. Rossini, V. Piccoli, U. Cornaro, J. Catal. 168 (1997) 334.
[48] J. Muslehiddinoglu, M.A. Vannice, J. Catal. 222 (2004) 214.
[49] H. Pines, W.O. Haag, J. Am. Chem. Soc. 82 (1960) 2471.
[50] S. Srinivasan, C.R. Narayanan, A. Biaglow, R. Gorte, A.K. Datye, Appl. Catal. A Gen. 132 (1995) 271.
[51] Z. Sarbak, Appl. Catal. A Gen. 159 (1997) 147.
[52] J. Haber, T. Machej, M. Derewinski, R. Janik, J. Krysciak, H. Sodowska, J. Janas, Catal. Today 54 (1999) 47.
[53] P.O. Scokart, A. Amin, C. Defosse, P.G. Rouxhet, J. Phys. Chem. 85 (1981) 1406.
[54] S. Srinivasan, C.R. Narayanan, A.K. Datye, Appl. Catal. A Gen. 132 (1995) 289.
[55] C. Otero Arean, B.S. Sintes, G.T. Palomino, C.M. Carbonell, E.E. Platero, J.B.P. Soto, Microporous Mater. 8 (1997) 187.
[56] H. Zou, J. Shen, Thermochim. Acta 351 (2000) 165.
[57] M.H. Lee, C.-F. Cheng, V. Heine, J. Klinowski, Chem. Phys. Lett. 265 (1997) 673.
[58] R.W. Grimes, A.B. Anderson, A.H. Heuer, J. Am. Chem. Soc. 111 (1989).
[59] P.M. Boorman, R.A. Kydd, Z. Sarbak, A. Somogyvari, J. Catal. 96 (1985) 115.
[60] A. Corma, V. Fornés, Appl. Catal. 61 (1990) 175.
[61] L.M. Rodriguez, J. Alcaraz, M. Hernandez, M. Dufaux, Y.B. Taarit, M. Vrinat, Appl. Catal. A Gen. 189 (1999) 53.
[62] A. Corma, H. Garcia, Chem. Rev. 103 (2003) 4307.
[63] L.M. Rodriguez, J. Alcaraz, M. Hernandez, Y.B. Taarit, M. Vrinat, Appl. Catal. A Gen. 169 (1998) 15.
[64] A. Davydov, Molecular Spectroscopy of Oxide Catalysts Surfaces, Wiley, Chichester, 2003.
[65] B.H. Davis, B. Shi, J. Catal. 157 (1995) 359.
[66] A. Gervasini, G. Belusi, J. Fenyvesi, A. Auroux, J. Phys. Chem. 99 (1995) 5117.
[67] H. Knözinger, A. Scheglila, J. Catal. 17 (1970) 252.
[68] B. Shi, H.A. Dabbagh, B.H. Davis, J. Mol. Catal. A Chem. 141 (1999) 257.
[69] M.A. Abdel-Rehim, A.C.B. dos Santos, V.L.L. Camorim, J.A. da Costa Faro, Appl. Catal. A Gen. 305 (2006) 211.